Solid State Communications 151 (2011) 1248–1251

Contents lists available at ScienceDirect

Solid State Communications

journal homepage: www.elsevier.com/locate/ssc

Hybrid AMR/PHR ring sensor

Sunjong Oh [a], P.B. Patil [a], Tran Quang Hung [a], Byunghwa Lim [a], Migaku Takahashi [a], Dong Young Kim [b], CheolGi Kim [a,*]

[a] Center for NanoBioengineering and Spintronics & Department of Materials Science and Engineering, Chungnam National University, Daejeon 305-764, Republic of Korea
[b] Department of Physics, Andong National University, Andong 760-749, Republic of Korea

ARTICLE INFO

Article history:
Received 26 May 2011
Accepted 29 May 2011
by A.H. MacDonald
Available online 12 June 2011

Keywords:
A. Magnetic films and multilayers
A. Thin film
D. Electronic transport

ABSTRACT

The AMR (anisotropic magnetoresistance) and PHR (planar Hall resistance) contribution was analyzed for fabricated ring type sensor junctions in single and multiring bridge sensors, and their field sensitivity was examined. The voltage profile, i.e. the sum of AMR and PHR effects, reveal anti-symmetric behavior with the magnetic field with small offsets due to the self-balancing of ring arm resistances, but the voltage variations for the external field are additive for all junction components. The field sensitivity of the resistance for a single ring sensor is 9.5 mΩ/Oe, and its value monotonously increased to 102.6 mΩ/Oe for 17 rings with an enhanced active area.

© 2011 Elsevier Ltd. All rights reserved.

1. Introduction

Recently, there have been large studies on the performance of micron size magnetic sensors to analyze bio-analytes with intermediation of biofunctionalized magnetic labels in 1-, 2-dimensional bioassay platforms [1–3]. Several kinds of magnetic sensors have been used in the past based on anisotropic magnetoresistance (AMR) [4], giant magnetoresistance (GMR) [5], magnetic tunnel junctions (MTJ) [6], micro-Hall sensors [7], and planar Hall resistance (PHR) [8,9] for immunomagnetic analysis. Each of these sensors has been marked by certain advantages and disadvantages.

A magnetic sensor can detect magnetic labels very efficiently down to single labels, when the sensor size is comparable with that of label, which is positioned over the sensor surface at a close proximity [10,11]. However, there is a possibility that submicron size sensors are not able to measure the average quantity of biofunctionalized labels which are randomly dispersed in sample volumes on the order of a few hundred micrometers. Therefore, it is desirable to develop an enlarged active sensing area of a few hundred microns, which is capable of measuring the ensemble average of bio-analytes in a sample volume.

In this letter, we have designed and fabricated a ring type bridge utilizing hybrid AMR–PHR effects for the enhancement of the field sensitivity and active area of a sensor. The role of AMR and PHR contribution from the bridge device elements was analyzed, and the field sensitivity was examined for the fabricated multiring bridges.

2. Experimental details

To realize a hybrid AMR–PHR junction device, we designed and fabricated the ring structure shown in Fig. 1. The spin-valve structure of Ta(3)/NiFe(10)/Cu(1.2)/NiFe(2)/IrMn(10)/Ta(3) (nm) was deposited to induce small interlayer exchange coupling between pinned and free magnetic layers and to enhance the field sensitivity of the hybrid AMR/PHR ring sensor. The 300 μm diameter ring junction device was prepared by a standard photolithographic technique and lift off process. The ring junction was connected with Ta(10 nm)/Au(80 nm) electrodes, as denoted by terminals A–D in Fig. 1(a) and (c), to lead the sensor contacts to the wire bonding pads at the edge of the chip. The change of the output voltage in electrodes C and D with the applied magnetic field, H_{app}, was measured for a fixed current of $I = 1$ mA through electrodes A and B.

Based on vector Ohm's equation, the AMR and PHR effect is related to diagonal and off-diagonal components in a resistivity tensor, respectively [12,13]. By considering the configuration of current and voltage electrodes, magnetic resistance arms in Fig. 1(a) are responsible for the AMR effect, whereas the square regions in Fig. 1(b) are responsible for the PHR effect. The equivalent circuit for each part, denoted by $R_1 \sim R_4$ for AMR and $R'_1 \sim R'_4$ for PHR, is depicted in Fig. 1(c).

* Corresponding author. Tel.: +82 42 821 6632; fax: +82 42 822 6272.
E-mail address: cgkim@cnu.ac.kr (C. Kim).

0038-1098/$ – see front matter © 2011 Elsevier Ltd. All rights reserved.
doi:10.1016/j.ssc.2011.05.049

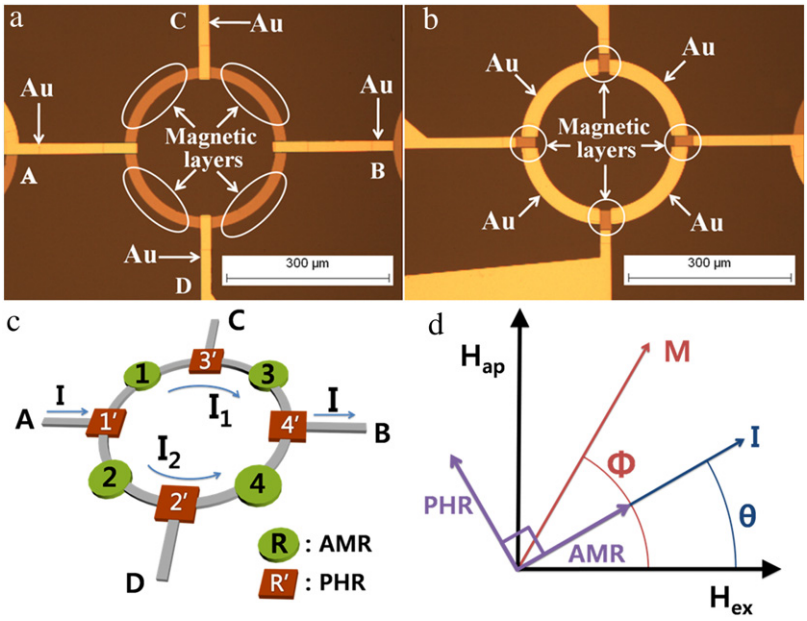

Fig. 1. (a) Arms of the ring contribute to the AMR components, (b) Square regions contribute to the PHR components, (c) Schematic representation showing parts of the ring contributing to AMR (R) and PHR (R') and (d) The coordinates defining magnetization and current direction. Here, θ and ϕ are the angles of the current direction and magnetization from the exchange biased direction, H_{ex}, respectively. Hap is the applied field.

3. Result and discussion

In order to understand the mechanism of our sensor, we consider single ring sensor. Both the AMR and PHR characteristics are analyzed by considering both the change in magnetization direction by the applied magnetic field and the current direction at each point of the arms along the ring curvature. The current angle θ depends on the position in the arms and so the resistance is integration of the current angle θ over the arm curvature. The magnetization direction ϕ with respect to reference direction (exchange biased direction H_{ex}), as shown in Fig. 1(d), can be determined by the equilibrium state of magnetization under the magnetic field and it will have the same value at all the points over arm curvatures if we neglect the edge effect in the arms.

At the given angle θ and ϕ as in Fig. 1(d), the output voltage by the AMR effect in the magnetic thin film is a function of $\cos^2(\phi - \theta)$ [14]. The output voltage from arm 1 is written as,

$$V_1 = \frac{\pi r I}{2tW}\left(\rho_\perp + \frac{2\Delta\rho}{\pi}\int_{\pi/2}^{0}\cos^2(\phi-\theta)\mathrm{d}\theta\right) \quad (1)$$

where r, W, and t are the radius, width, and thickness of the ferromagnetic film, respectively, and $\Delta\rho = \rho_{11} - \rho_\perp$ with $\rho_\perp$ and ρ_{11} representing the electrical resistivity values when the directions of the magnetization and current are perpendicular and parallel, respectively. The Output voltages V_2, V_3, and V_4 for arms 2, 3, and 4 are obtained by changing the range of integration of Eq. (1) such as $V_2 \sim \int_{3\pi/2}^{2\pi}$, $V_3 \sim \int_{2\pi}^{3\pi/2}$, $V_4 \sim \int_{0}^{\pi/2}$, respectively. The output voltage by the AMR has an offset voltage determined by a resistance value of $\rho_\perp$.

Whereas the output voltage by PHR has no offset value and is described by the function of $\sin(\phi - \theta)\cos(\phi - \theta)$ [15]. The horizontal current component for the square regions of Fig. 1(b) contributes to the PHR effect, assigning the current angle $\theta = 0$ for all square regions. So, the output voltage from the square region PHR effect can be written by setting $\theta = 0$ as,

$$V_1' = V_2' = V_3' = V_4' = \frac{I\Delta\rho}{t}\sin(\phi)\cdot\cos(\phi). \quad (2)$$

As for the calculation of the voltage profile using Eqs. (1) and (2), the magnetization angle $\phi(H)$ with the applied field was obtained from the Stoner–Wohlfarth model [16].

For the bridge circuit of AMR arms of $R_1 \sim R_4$, the voltage between terminals C and D is governed by the average of the unbalanced voltages of (V_1 and V_2) and (V_3 and V_4), giving the output voltage of $((V_1+V_4)-(V_2+V_3))/2$ [14]. In order to examine the role of each AMR arms, the magnetic parts of selective arms and PHR squares were replaced by Au electrode elements to get rid of their contributions as shown in Fig. 2. Fig. 2(a)–(c) show the comparison of measured voltage profiles with calculated ones for different configurations of AMR arms. Here, we used 2% of the AMR ratio of NiFe thin films with a resistivity $\rho = 19.3\times10^{-8}$ Ωm in the profile calculation shown as insets of Fig. 2(a)–(c) and the reported material parameters in the spin-valve structure [16]. There is good agreement in the shapes and relative offset voltages between the measured and calculated voltage profiles for different Au electrode configurations.

The voltage profiles of V_1 and V_4 were calculated to have identical variation tendencies with the field, but opposite to those of V_2 and V_3. When facing arms R_2 and R_3 are replaced by Au, the output voltage results only from V_1 and V_4 because R_2 and R_3 are zero as shown in Fig. 2(a). We can see a large offset voltage due to $\rho_\perp$ in the AMR effect and an asymmetric behavior with respect to field $H = 0$ in both measured and calculated profiles. In Fig. 2(b), one arm of R_3 is replaced by the Au electrode, resulting in $V_2 = 0$. Also, a relatively large offset voltage and asymmetric behavior were revealed in both the measured and calculated voltage profiles.

With all AMR arms, as in Fig. 2(c), the output voltage reveals an anti-symmetric profile with a very small offset voltage. This indicates that the offset voltage of each arm was canceled out due to self-balancing of the four AMR arms, but the voltage variations of each arm with the external fields are additive because the variation tendencies of V_1 and V_4 for an external field are opposite to those of V_2 and V_3. The observed small offset voltage is due to the different resistance values of $R_1 \sim R_4$ due to the imperfect lithography process.

Fig. 3 shows the decomposition of AMR and PHR contribution due to the four AMR arms and PHR elements, respectively. The

Download English Version:

https://daneshyari.com/en/article/1593215

Download Persian Version:

https://daneshyari.com/article/1593215

Daneshyari.com